UNIVERSITÀ DEGLI STUDI DI PADOVA

Department of Biomedical Science

Interuniversity Bachelor's degree programme
in Biology of Human and Environmental Health

Final dissertation

INVESTIGATING THE ROLE OF *GBA1* and *LIMP2* IN LIPID HOMEOSTASIS: IMPLICATIONS FOR LYSOSOMAL DYSFUNCTION and NEURODEGENERATION

Supervisor: Prof. Francesco Argenton
Co-Supervisor: Prof. Nicoletta Plotegher

Candidate: Eda Ugurlar
Student ID number: 2105808

ACADEMIC YEAR 2025/2026

Abstract

Lysosomal dysfunction and altered lipid metabolism are increasingly recognised as key contributors to neurodegenerative disorders, including Parkinson's disease. Mutations in *GBA1*, encoding the lysosomal enzyme β-glucocerebrosidase (GCase), represent the strongest genetic risk factor for Parkinson's disease and are associated with impaired lysosomal lipid degradation. GCase trafficking to the lysosome depends on the lysosomal integral membrane protein type-2 (*LIMP-2*), encoded by *SCARB2*. However, the contribution of *GBA1* and *LIMP-2* dysfunction to lipid-droplet homeostasis remains incompletely understood.

This study investigated the roles of *GBA1* and *LIMP-2* in cellular lipid homeostasis using wild-type, *GBA1*-knockout (11F) and *SCARB2*-knockout (F6) HEK293 cells, characterised in parallel by Western blotting (PLIN2, *GBA1*, LAMP1), BODIPY-based lipid-droplet imaging, and targeted lipidomics by liquid chromatography–mass spectrometry.

The two knockouts produced distinct, mechanism-specific alterations in lipid-droplet biology. *GBA1* deficiency was associated with accumulation of glucosyl/galactosylceramides and glucosylated cholesterol, together with significantly smaller lipid droplets, reduced triglycerides and lower PLIN2, consistent with loss of GCase hydrolytic activity. In contrast, *LIMP-2* deficiency drove an increase in lipid-droplet number enriched in free cholesterol and cholesteryl esters, with the lowest PLIN2 and triglyceride levels, consistent with the GCase-independent role of *LIMP-2* in lysosomal cholesterol export.

Together, these findings indicate that *GBA1* and *LIMP-2* contribute to lipid-droplet homeostasis through GCase-dependent and GCase-independent pathways, respectively, providing mechanistic insight into how lysosomal dysfunction reshapes cellular lipid storage in Gaucher disease and *GBA1*-associated neurodegeneration.

Key words: Lipid homeostasis, Lysosome, Neurodegeneration, *GBA1*, *LIMP2* (SCARB2)

1. Introduction

1.1 Lysosomal Function and the Role of *GBA1* in Health and Disease

Lysosomes are intracellular organelles traditionally recognised as the cell's primary disposal and recycling centres, but more recent work has established them as key metabolic hubs that coordinate growth, energy management and nutrient sensing. Lysosomes contain more than 60 soluble hydrolases and accessory proteins, together with numerous membrane-associated and transiently localised proteins (1) Most lysosomal enzymes reach the organelle via the mannose-6-phosphate receptor pathway, but β-glucocerebrosidase (GCase) is a notable exception that depends on the lysosomal integral membrane protein type-2 (LIMP-2) as a specific trafficking receptor. The GCase–LIMP-2 complex forms in the endoplasmic reticulum and is co-transported through the Golgi to the lysosome, defining a mannose-6-phosphate-independent trafficking route. (2)

Dysfunction of lysosomal proteins causes lysosomal storage disorders (LSDs), which collectively affect more than 1 in 5,000 live births. (3) Among the enzymes involved, β-glucocerebrosidase (GCase), encoded by *GBA1*, is a lysosomal glycosidase that hydrolyses glucosylceramide (GlcCer) into glucose and ceramide. More than 500 *GBA*1 mutations have been identified, many of which impair protein folding, stability or catalytic function and lead to reduced lysosomal GCase activity through defective trafficking and/or decreased enzymatic efficiency. (4) Reduced GCase activity results in GlcCer accumulation and subsequent buildup of its deacylated form glucosylsphingosine (GlcSph) within lysosomes, with adverse consequences for lysosomal function and cell health. (4)

Biallelic mutations in *GBA1* cause Gaucher disease (GD), which spans a range of clinical severities. The most severe neuronopathic form, GD type 2, arises from null or highly deleterious mutations and is typically fatal in infancy, with no effective disease-modifying treatments available. (5) GD type 3 is a chronic neuronopathic form with milder neurological manifestations and survival beyond infancy. (5) GD is the most common sphingolipidosis, and both homozygous and heterozygous *GBA1* mutation carriers have an increased risk of Parkinson's disease (PD) and dementia with Lewy bodies (DLB). *GBA1*-associated PD is neuropathologically similar to sporadic PD but often shows earlier onset, more severe non-motor symptoms and faster progression. (6,7)

These observations support the idea that therapeutic strategies aimed at restoring GCase activity and lysosomal function could benefit Gaucher disease and related neurodegenerative conditions. *GBA1* variants are present in approximately 3–25% of PD patients, depending on the considered population

and represent the strongest known genetic risk factor for the disease. (6,7) Reduced GCase activity has also been reported in sporadic and non-*GBA1* genetic forms of PD, suggesting that lysosomal GCase dysfunction may constitute a broader pathogenic mechanism in neurodegeneration. (7) Pathogenic *GBA1* mutations such as L444P and N370S produce misfolded GCase with markedly reduced enzymatic activity, typically around 10–20% of normal, leading to glycosphingolipid accumulation that characterises GD and is thought to contribute to PD-related neurodegenerative processes. (6)

Given these shared genetic and molecular mechanisms, enhancing lysosomal GCase activity in the brain is a promising strategy to restore lysosomal function and re-establish cellular homeostasis in neuronopathic Gaucher disease and *GBA1*-associated neurodegenerative disorders. Structural studies of the GCase–LIMP-2 complex have revealed a hydrophobic interaction interface supported by key residues and salt bridges that are essential for correct trafficking and enzymatic function. (2)

1.2 Structural basis of GCase–LIMP-2 interaction

The interaction between β-glucocerebrosidase (GCase) and its lysosomal transporter LIMP-2 is mediated by specific structural domains that ensure proper trafficking and enzymatic regulation. (see **Scheme 1**) On LIMP-2, the binding interface consists of a hydrophobic three-helix bundle, with helix 5 and helix 7 playing a critical role in GCase recognition. (8) Correspondingly, GCase presents a complementary hydrophobic binding surface formed by helices 1a, 1b, and 2, enabling stable complex formation through hydrophobic interactions. The integrity of this hydrophobic interface is essential for proper protein interaction. Mutations that disrupt hydrophobicity within these regions, for example through the introduction of charged amino acids, impair LIMP-2 binding and consequently hinder the trafficking of GCase to the lysosome. (9)

Importantly, the interaction between GCase and LIMP-2 is regulated in a pH-dependent manner. Binding occurs in the endoplasmic reticulum under neutral pH conditions, where the complex is formed and transported through the secretory pathway. Upon arrival in the lysosome, the acidic environment (pH ~4.5–5.0) induces conformational changes in the LIMP-2 binding site, promoting dissociation of the complex. This process allows GCase to be released as an active enzyme within the lysosomal lumen. (4)

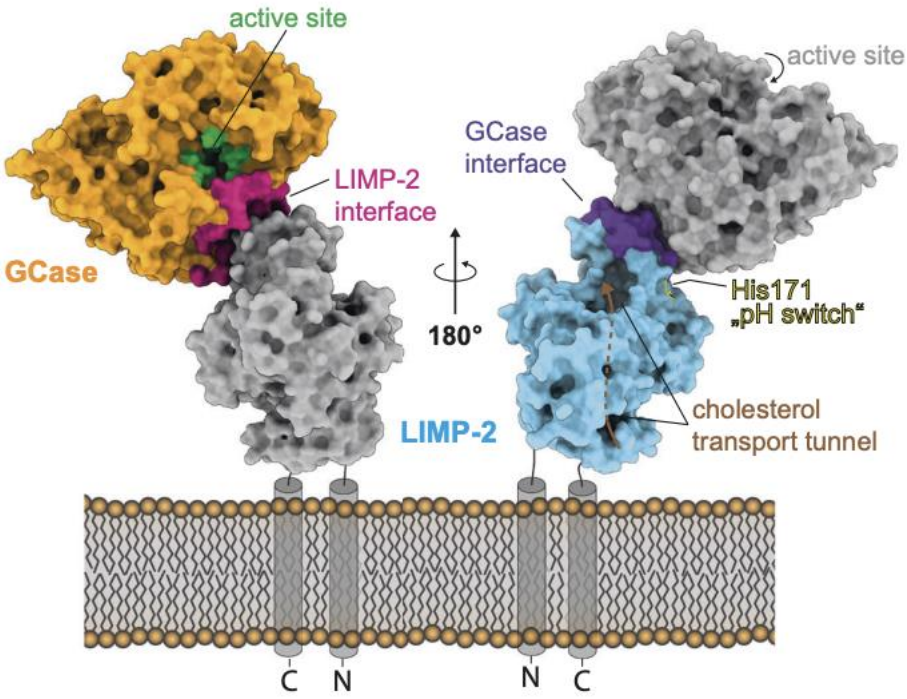

Scheme 1. Architecture of the GCase/LIMP-2 complex at the lysosomal membrane, showing the active site, the GCase–LIMP-2 interaction interface, the pH-sensitive His171 switch, and the LIMP-2 cholesterol transport tunnel. Adapted from Dobert et al., 2025 (2), published under a CC BY 4.0 license.

Notably, helix 5 of LIMP-2 alone has been shown to be sufficient for GCase binding, provided that its hydrophobic character and helical structure are preserved. In addition to its role in trafficking, the interaction between LIMP-2 and GCase also contributes to the regulation of GCase enzymatic activity. Following dissociation in the lysosome, full catalytic activation of GCase is primarily mediated by saposin C, which facilitates substrate access and optimal enzymatic function. (9) In addition to its trafficking role, LIMP-2 also contributes to lysosomal lipid handling (see below). Taken together, these findings highlight the central role of *GBA1* and LIMP-2 in lysosomal function and lipid metabolism; however, while their involvement in lysosomal lipid degradation is well established, their potential role in regulating lipid-droplet homeostasis remains less clearly defined. (10)

1.3 Beyond GCase trafficking: lipid-handling functions of LIMP-2

Beyond its role as a GCase chaperone, LIMP-2 also contributes directly to lysosomal lipid handling. Its luminal cavity binds and exports cholesterol from the lysosome to acceptor organelles including lipid droplets (see **Scheme 1**), and its depletion disrupts cellular cholesterol regulation (11); LIMP-2

has additionally been identified as a component of lysosome–ER membrane contact sites involved in inter-organelle lipid transfer. (10) These GCase-independent activities place LIMP-2 at the intersection of cholesterol distribution and lipid-droplet composition.

1.4 *GBA1–GBA2* cross-talk and transglucosylation

GCase activity is not isolated within the cell: the non-lysosomal β-glucosidase *GBA2* also hydrolyses glucosylceramide, and the two enzymes show substrate-level cross-talk, with *GBA2* partially compensating when GCase activity is lost. (12) Beyond glycosphingolipid turnover, β-glucosidases including GCase and *GBA2* can also transfer a sugar between glycosphingolipids and cholesterol to generate glycosylated cholesterol species. (13) Loss of GCase activity may therefore perturb not only glycosphingolipid catabolism but also the glycosylation of sterols.

1.5 Lipid droplets and their coupling to the lysosome

Lipid droplets (LDs) are dynamic, ubiquitous organelles consisting of a neutral-lipid core, primarily triacylglycerols (TAG) and cholesteryl esters (CE), surrounded by a phospholipid monolayer decorated with specialised coat proteins of the perilipin (PLIN) family. PLIN2 is constitutively associated with LDs in most cell types, protects them from lipolytic turnover and, in many systems, its abundance broadly correlates with cellular neutral-lipid content. (14) Far from being inert storage depots, LDs participate in lipid signalling, membrane biogenesis and energy homeostasis, and they communicate with multiple organelles, including the lysosome. The selective degradation of LDs by lysosomes via autophagy, i.e. lipophagy, represents a major route by which stored neutral lipids are mobilised, and links LD turnover directly to lysosomal function. Lysosomal dysfunction is therefore expected to affect not only lipid catabolism within lysosomes but also the size, composition and turnover of the cellular LD pool.

1.6 Knowledge gap

Despite extensive research on lysosomal function and lipid metabolism, the link between lysosomal dysfunction and lipid droplet homeostasis remains incompletely understood. While *GBA1* and *LIMP-2* are known to play key roles in lysosomal lipid degradation, their impact on lipid droplet accumulation, turnover and interaction with lysosomes has not been fully elucidated. In particular, whether the GCase-dependent and GCase-independent functions of the GCase–*LIMP-2* axis act on

the same or on distinct branches of lipid-droplet biology has not been directly tested in a controlled cellular system.

Furthermore, although lipophagy represents a central pathway connecting lipid droplets to lysosomal degradation, it remains unclear how defects in *GBA1*- or *LIMP-2*-dependent lysosomal function influence lipid droplet–lysosome coupling and lipophagic activity.

1.7 Hypothesis

Based on the central role of *GBA1* and *LIMP-2* in lysosomal function and lipid metabolism, and on the distinct biochemical activities of the two proteins outlined above, we hypothesise that the loss of *GBA1* or *LIMP-2* perturbs lipid-droplet homeostasis through distinct, mechanism-specific pathways. Specifically, loss of GCase activity is expected to disrupt glycosphingolipid catabolism and, secondarily, neutral-lipid storage, whereas loss of *LIMP-2* is expected to impair cholesterol export and alter the composition of the lipid-droplet pool independently of GCase activity. The two perturbations are therefore predicted to produce qualitatively different rather than uniformly increased lipid droplet phenotypes.

To test this hypothesis, this study quantitatively assesses lipid-droplet accumulation in *GBA1*- and *LIMP-2*-deficient HEK293 cells using fluorescence imaging combined with Western blot analysis of lipid-droplet (PLIN2) and lysosomal (LAMP1) markers. A comparative analysis is performed to determine whether the loss of *GBA1* and *LIMP-2* differentially affects lipid-droplet burden and the underlying lipidome. To resolve the molecular composition of these alterations, targeted lipidomics by liquid chromatography mass spectrometry is used to profile the major sphingolipid, glycerolipid and sterol species across genotypes. Together, these approaches aim to provide mechanistic insight into how lysosomal dysfunction influences lipid-droplet dynamics and to define the distinct contributions of *GBA1* and *LIMP-2* to the maintenance of cellular lipid homeostasis.

2. Materials and Methods

2.1 Cell lines and culture conditions

Human embryonic kidney (HEK293) cells were used, including wild-type (WT), CRISPR/Cas9-generated *GBA1* knockout (11F) and *SCARB2* knockout (*LIMP-2*-deficient, F6) lines. Cells were maintained under standard conditions at 37 °C in a humidified incubator with 5% CO_2.

Cells were cultured in Dulbecco's Modified Eagle Medium (DMEM) supplemented with fetal bovine serum (FBS, 10%) and penicillin/streptomycin (PEN/STREP, 1%). Cells were routinely passaged to maintain sub-confluent conditions.

2.2 Western blot analysis

WT, 11F and F6 HEK293 cells were centrifuged at 500 × *g* for 5 minutes. The pellets were lysed using RIPA buffer (40 µL) supplemented with protease inhibitors (1× final concentration). Lysates were incubated on ice for 30 minutes and centrifuged at 21,000 × *g* for 30 minutes at 4 °C. Supernatants were collected for downstream analysis.

Protein concentrations were determined using the bicinchoninic acid (BCA) assay, with bovine serum albumin (BSA) as standard. Both samples and BSA were prepared in duplicate in a 96-well plate and incubated at 37 °C for 30 minutes. Absorbance was measured at 560 nm and protein concentration was calculated using a BSA standard curve.

Equal amounts of protein (35 µg per sample) were mixed with SDS-containing sample buffer supplemented with reducing agents and separated by SDS-PAGE at 150 V. Proteins were transferred onto PVDF membranes pre-activated in methanol. Membranes were blocked in blocking solution (TBST + 5% non-fat dried milk) for 1 hour at room temperature and subsequently incubated overnight at 4 °C with the following primary antibodies prepared in blocking solution:

- rabbit anti-PLIN2 (1:1000) — lipid-droplet marker (45–48 kDa)
- rabbit anti-GBA1 (1:1000) — lysosomal glucocerebrosidase marker (60 kDa)
- rabbit anti-LIMP-2 (1:1000) — *GBA1* trafficking receptor marker (55 kDa)
- rabbit anti-LAMP1 (1:500) — lysosomal marker (100 kDa)
- mouse anti-β-actin (1:10000) — loading control (43 kDa)

After overnight incubation, membranes were washed three times in TBST and incubated with appropriate HRP-conjugated secondary antibodies for 1 hour at room temperature, diluted in blocking solution as follows:

- Anti-rabbit (1:16000)
- Anti-mouse (1:80000)

Signal detection was performed using the ChemiDoc™ imaging system with Immobilon™ Forte substrate, which reacts with the horseradish peroxidase (HRP) conjugated to the secondary antibodies, producing a luminescent signal proportional to the amount of protein present.

2.3 Immunocytochemistry and fluorescence imaging

WT, 11F and F6 HEK293 cells were counted using Trypan blue exclusion and seeded at a density of 5×10^4 cells per well in 24-well plates containing glass coverslips for immunocytochemistry.

Cells grown on coverslips were fixed with 4% paraformaldehyde for 30 minutes at room temperature, followed by three washes with PBS. Cells were permeabilised in PBS containing 0.1% Triton X-100 for 20 minutes and subsequently washed with PBS. Blocking was performed using PBS supplemented with 5% fetal bovine serum (FBS) for 1 hour at room temperature.

For lipid staining, cells were incubated with BODIPY 493/503 (10 µM working concentration; excitation peak at 493 nm, emission peak at 503 nm) for 30 minutes at 37 °C in the dark, followed by washing with PBS.

Nuclei were stained with DAPI (1:10000 in deionised H_2O) for 5 minutes, followed by three washes with PBS. Coverslips were mounted onto glass slides using Mowiol mounting medium and stored in the dark at 4 °C until imaging.

Fluorescence images were acquired using a ZEISS fluorescence microscope equipped with a 63× objective. For each sample, DAPI (nuclei, blue) and BODIPY (lipid droplets, green) channels were captured, and representative images were obtained for each experimental condition. Acquisition parameters (exposure time, gain and laser/lamp intensity) were kept constant across all samples within a given experiment to allow quantitative comparison.

2.4 Targeted lipidomics by liquid chromatography–mass spectrometry

Lipidomic profiling of WT, 11F and F6 HEK293 cells was performed to quantify the relative abundance of major sphingolipid, glycerolipid and sterol species and was carried out in collaboration with Ca' Foscari University of Venice. Lipids were extracted from cells using the classical Folch extraction method. Lipidomic profiling was performed using a Cyclic Ion Mobility mass spectrometer (Waters), acquired with MassLynx software, and data evaluation was performed using LipoStar software. The various steps of the process were performed by Dr Laura Pagnin and Dr Alessandro

Bonetto (Department of Environmental Sciences, Informatics and Statistics, Ca' Foscari University of Venice) in the laboratory of Prof. Antonio Marcomini.

2.5 Data analysis and statistics

Western blot band intensities were quantified by densitometry using Fiji software. For each blot, the signal of the target protein was normalised to the corresponding β-actin loading-control band; values from independent biological replicates were then expressed either relative to β-actin or as fold change relative to CTRL, as indicated in the figure legends. Results are presented as mean ± SD with individual replicate values overlaid; the number of independent biological replicates (*n*) is reported in each figure legend. Comparisons between WT, 11F and F6 were made by one-way ANOVA followed by Tukey's or Dunnett's multiple-comparison test, as appropriate, using GraphPad Prism.

Fluorescence images were analysed in FIJI/ImageJ. After background subtraction and intensity thresholding of the BODIPY channel under conditions held constant across genotypes, lipid droplets were segmented using the Analyse Particles function. To avoid pseudoreplication, inferential statistics on lipid-droplet morphometry were performed exclusively on per-image (replicate-level) summary values, using the same one-way ANOVA framework described above.

For the lipidomic data, the targeted species intensities reported in this work are descriptive (mean area ± SD across biological replicates) and were not subjected to formal between-group inferential statistics; where genotype effects are discussed, they are reported as consistent trends, with the magnitude and variability of each species shown in the corresponding figures.

3. Results

To investigate the contribution of GBA1 and LIMP-2 to cellular lipid homeostasis, wild-type (WT/CTRL), *GBA1*-KO (11F) and *SCARB2*-KO (F6) HEK293 cells were characterised by Western blotting, lipid-droplet imaging and targeted lipidomics. The three approaches were designed to be complementary: protein expression reported on the lysosomal and lipid-droplet machinery, fluorescence imaging quantified lipid-droplet number and morphology, and mass spectrometry resolved the underlying lipid species. Western blot and imaging analyses were performed on three independent biological replicates per condition and were compared by one-way ANOVA with multiple-comparison correction; lipidomic data are reported as relative signal intensities rather than absolute concentrations.

3.1 Validation of the knockout models by Western blot

Western blot analysis confirmed the expected genotypes. (**Figure 1**) GBA1 protein was visually undetectable in 11F cells and quantified at ≈0.01 relative to β-actin, against ≈0.85 in CTRL and ≈1.2 in F6 cells; the 11F-versus-CTRL difference did not reach formal statistical significance with n = 3 ($p > 0.05$), most likely owing to the variability of the CTRL signal, but a significant difference was observed between 11F and F6 ($p < 0.05$). The visual absence of the GBA1 band in 11F confirms a functional loss of GCase. In F6 cells, total GBA1 was comparable to control, indicating that loss of LIMP-2 does not reduce the overall amount of GCase protein. β-actin signal was uniform across genotypes, confirming equal loading.

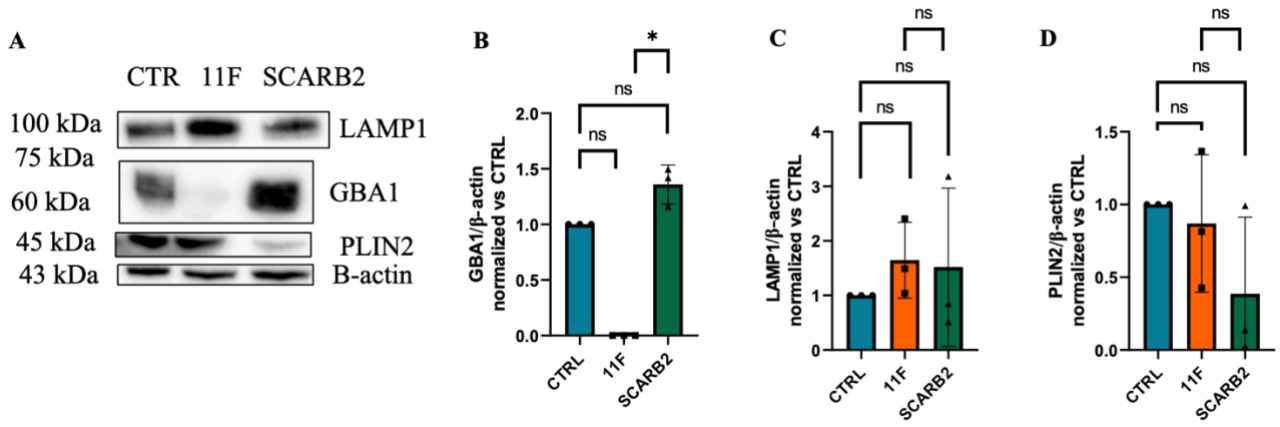

Figure 1. Western blot validation of the knockout models. (A) Representative immunoblots of whole-cell lysates from wild-type (CTRL), GBA1-knockout (11F) and SCARB2-knockout (SCARB2) HEK293 cells, probed for LAMP1 (100 kDa), GBA1 (60 kDa) and PLIN2 (45 kDa), with β-actin (43 kDa) as loading control. Densitometric quantification of (B) GBA1, (C) LAMP1 and (D) PLIN2, each normalised to β-actin and expressed relative to CTRL. Bars represent mean ± SD with individual biological replicates overlaid (n = 3); groups were compared by one-way ANOVA with multiple-comparison correction.

* $p < 0.05$; ns, not significant.

LAMP1, a lysosomal membrane marker, was modestly increased in both mutant lines relative to control (≈1.5–1.6× CTRL), with no substantial difference between 11F and F6. None of the pairwise comparisons reached statistical significance (n = 3, $p > 0.05$), so this increase is reported as a consistent trend rather than a statistically robust difference.

LIMP-2 protein expression could not be reliably assessed by Western blot in this study: the LIMP-2 immunoblot was affected by contamination of the F6 lane by WT signal, which prevented a valid

comparison between genotypes, and this blot was therefore excluded from quantification. Consequently, F6' s identity as a *SCARB2* knockout rests on the CRISPR/Cas9 editing strategy used to generate the line and is functionally supported by its distinctive lipidomic phenotype (accumulation of free cholesterol and cholesteryl esters; Section 4.3), consistent with loss of the cholesterol-export function of LIMP-2.

PLIN2, the principal lipid-droplet coat protein examined here, showed a stepwise reduction across genotypes by densitometry, being highest in CTRL (≈1.3 relative to β-actin), intermediate in 11F (≈0.9) and lowest in F6 (≈0.4). None of the pairwise comparisons reached formal statistical significance with n = 3, owing to substantial inter-replicate variability — particularly in CTRL — so this gradient is reported here as a consistent directional trend rather than as a statistically significant difference

3.2 Lipid-droplet quantification by fluorescence imaging

Lipid droplets were visualised with BODIPY 493/503 and quantified for number, size, total and fractional area, perimeter and integrated density (**Figure 2**). The two mutant lines displayed opposite phenotypes. In 11F cells, several morphometric parameters were significantly reduced relative to control: average droplet size, perimeter and mean integrated density were all decreased ($p < 0.05$ in each case), indicating significantly smaller individual droplets. Droplet count, total area and fractional (%) area were also lower in 11F than in CTRL but did not reach formal statistical significance. (**Figure 2**) In contrast, F6 cells showed an increase in lipid-droplet number, total area and fractional area relative to CTRL, while the size, perimeter and integrated density of individual droplets remained within the control range. The F6-versus-CTRL comparisons did not reach statistical significance owing to substantial inter-replicate variability in F6; however, F6 differed significantly from 11F for droplet count, total area and fractional area ($p < 0.01$). In F6 cells, the higher lipid-droplet burden arose from a greater number of droplets that remained within the normal size range, rather than from enlargement of individual droplets, and this 'many-normal-droplets' phenotype was statistically distinct from the reduced-droplet phenotype observed in the GCase-deficient 11F line.

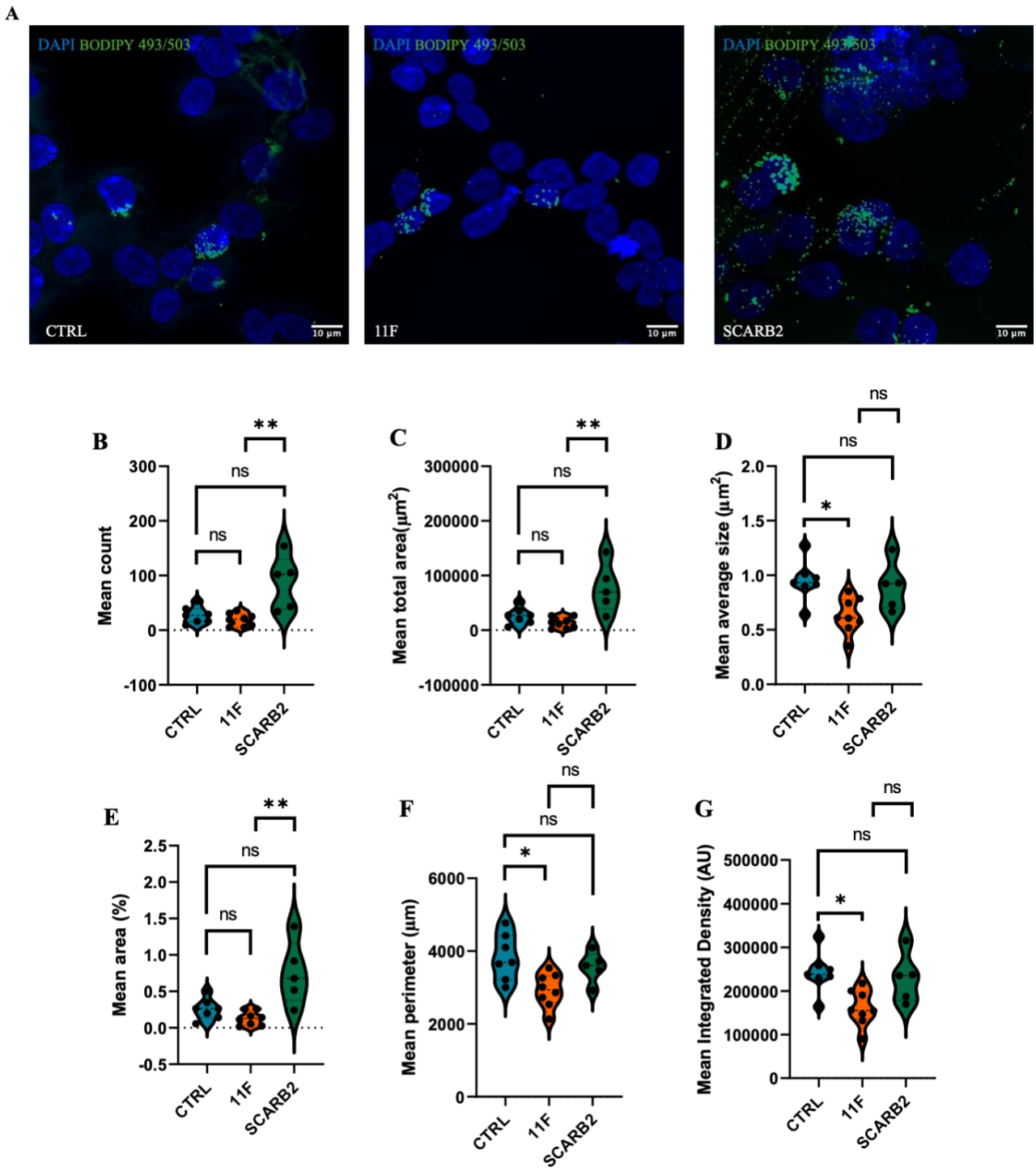

Figure 2. Lipid-droplet quantification by fluorescence imaging. (A) Representative fluorescence images of WT (CTRL), GBA1-knockout (11F) and SCARB2-knockout (F6) HEK293 cells stained with BODIPY 493/503 (green, lipid droplets) and DAPI (blue, nuclei). Images were acquired on a ZEISS fluorescence microscope with a 63× objective under identical acquisition settings across genotypes. Scale bar: 10 µm. (B-G) Quantification of lipid-droplet parameters from thresholded BODIPY images using FIJI: mean lipid droplet count (B) , mean total area (µm²) (C), mean average droplet size (µm²) (D), mean area fraction (%) (E), mean perimeter (µm) (F) and mean integrated density (AU, arbitrary units) (G). Violin plots show the

distribution of per-image values. Groups were compared by one-way ANOVA with multiple-comparison correction. * $p < 0.05$; ** $p < 0.01$; ns, not significant.

3.3 Lipidomic profiling of the knockout models

Targeted lipidomics by liquid chromatography–mass spectrometry resolved the lipid classes underlying the imaging and Western blot phenotypes. (**Figure 3**) The clearest single result was the accumulation of glucosyl/galactosylceramides in 11F cells, (**Figure 3**) which showed the highest intensities for several species (notably the 18:1/16:0 and 18:1/24:0 forms) and reproduced the pattern observed in an earlier analytical campaign. This substrate accumulation provides an independent biochemical confirmation that 11F is a functional GCase-deficient line.

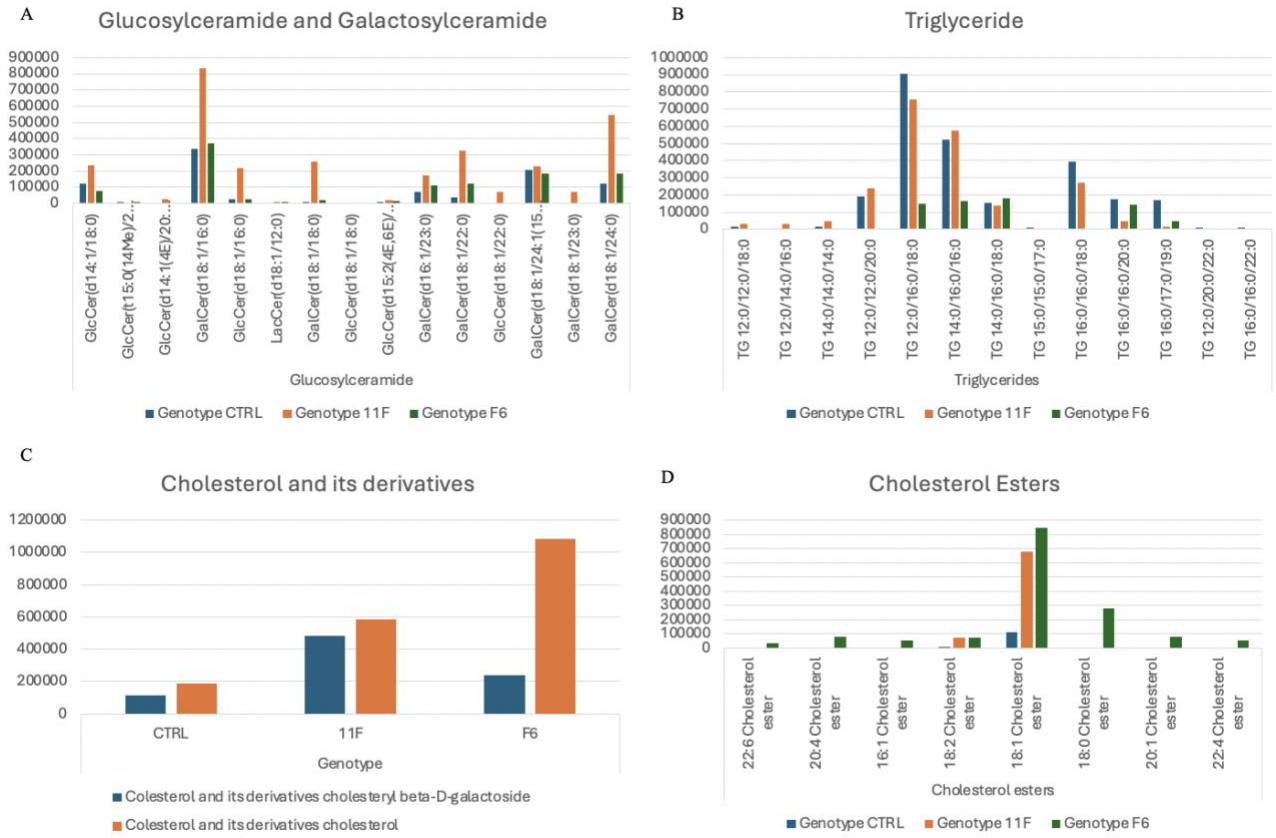

Figure 3. Targeted lipidomic profiling of the knockout models. Relative abundance of selected lipid classes measured by liquid chromatography–mass spectrometry in wild-type (CTRL, blue), *GBA1*-knockout (11F, orange) and SCARB2-knockout (F6, green) HEK293 cells: (A) glucosyl- and galactosylceramides; (B) triglycerides; (C) cholesterol and its derivatives (free cholesterol and glucosylated cholesterol); and (D)

cholesteryl (steryl) esters. Bars represent the mean signal intensity (peak area) across biological replicates; individual lipid species are indicated on the x-axis.

Triglycerides showed the opposite distribution (**Figure 3**): signal intensities were highest in control cells and lower in both mutants, with F6 displaying the lowest triglyceride content overall.

The cholesterol-related classes distinguished the two mutants most sharply. Free (unesterified) cholesterol was the highest in F6 cells, whereas glucosylated cholesterol (cholesteryl-β-D-glucosyl) was the highest in 11F. (**Figure 3**) Cholesteryl/steryl esters were markedly higher in F6 across essentially all acyl-chain lengths examined, mirroring the elevated free-cholesterol signal in the same line. Taken together, the lipidomic data indicate that the two knockouts perturb distinct branches of lipid metabolism: 11F is dominated by glycosphingolipid (GlcCer) and glycosylated-sterol accumulation, whereas F6 is dominated by cholesterol and cholesteryl-ester accumulation, with both lines showing reduced triglycerides.

4. Discussion

The combined biochemical, imaging and lipidomic data support a model in which GBA1 and LIMP-2 loss produce two mechanistically distinct lesions in lipid-droplet homeostasis. GCase deficiency (11F) reduced the size of individual lipid droplets and was accompanied by accumulation of its glycosphingolipid substrate, whereas LIMP-2 deficiency (F6) drove a cholesterol-centred lipid-droplet accumulation with the lowest coat-protein expression of the three genotypes. These phenotypes are consistent, respectively, with GCase-dependent and GCase-independent functions of the GCase–LIMP-2 axis.

4.1 GBA1 loss reduces lipid-droplet content and accumulates glycosphingolipids

The visual absence of the GBA1 band and the near-zero densitometric signal in 11F cells indicate that this line models a strong loss of GCase protein, in agreement with reports that pathogenic *GBA1* mutations markedly reduce GCase protein and activity. (15) Although the 11F-versus-CTRL densitometric difference did not reach formal significance with n = 3, the lipidomic accumulation of glucosyl/galactosylceramides in this line provides a substrate-level confirmation of GCase loss-of-function that is independent of antibody-based quantification. (15,16)

At the lipid-droplet level, 11F cells contained significantly smaller droplets and showed a trend toward a reduced overall burden, accompanied by lower PLIN2 expression because PLIN2 abundance correlates with cellular triacylglycerol (TAG) content and with lipid-droplet number. (14) Its reduction in 11F cells is consistent with the decreased triglyceride levels detected by lipidomics, suggesting a lower neutral-lipid storage load rather than altered coat-protein regulation. This interpretation is in line with previous reports showing that GCase deficiency impairs the uptake and storage of fatty acids into lipid droplets. (17) It should be noted, however, that the cell-type context matters: in human substantia nigra, experimental glycolipid disturbance produced cell-type-specific rather than uniform changes in neutral-lipid storage, (16) so the direction observed here should be regarded as model-dependent.

A further feature of the 11F lipidome was the accumulation of glucosylated cholesterol (cholesteryl-β-D-glucoside). The glycosylation of cholesterol into hexosyl-cholesterol species has been linked to perturbed glycosphingolipid metabolism, and its accumulation here parallels the buildup of glycosphingolipid substrates in the GCase-deficient line; the specific enzyme responsible for this glucosylated species in our system remains to be determined.

4.2 LIMP-2 loss drives a cholesterol-rich, PLIN2-low lipid-droplet accumulation

The F6 phenotype was, in several respects, the inverse of 11F. Loss of LIMP-2 did not reduce total GBA1 protein, consistent with the role of LIMP-2 in trafficking GCase to the lysosome rather than in controlling its synthesis; total enzyme levels can therefore appear normal or even slightly elevated even when lysosomal delivery is compromised. The defining feature of F6 was an increase in lipid-droplet number accompanied by the lowest PLIN2 expression of the three genotypes. This combination of increased droplet number, low PLIN2 and a cholesterol-centred lipid signature is in line with published LIMP-2/SCARB2-deficient models, where loss of LIMP-2 disrupts lysosomal cholesterol export and is associated with altered sterol storage and reduced triglyceride-based lipid stores . (11,18) Although the F6 increase in droplet number did not reach formal significance versus CTRL, it was significantly higher than in the GCase-deficient 11F line, and this combination — more droplets with the lowest coat-protein content — cannot be explained by a simple “more storage, more coat protein” relationship.

The lipidomic data resolve this apparent paradox. F6 cells accumulated free cholesterol and, in particular, cholesteryl esters across all chain lengths, while their triglyceride content was the lowest

of the three lines. The increased lipid-droplet population in F6 is therefore best interpreted as a cholesteryl-ester-enriched, triglyceride-poor droplet population. This is precisely the lipid signature predicted by the established function of LIMP-2 in lysosomal cholesterol export: the luminal cavity of LIMP-2 binds and delivers cholesterol to the lysosomal membrane and subsequently to lipid droplets, and depletion of LIMP-2 disrupts this efflux and the associated sterol-regulatory feedback. (11) When cholesterol cannot be exported normally, its esterification and deposition into lipid droplets offers a plausible route to the cholesteryl-ester accumulation observed here. The recently described participation of LIMP-2 in lysosome–endoplasmic reticulum contact sites provides a further, complementary mechanism by which its loss could perturb inter-organelle lipid transfer and droplet composition. (10)

The dissociation between droplet number and PLIN2 content is itself informative. PLIN2 preferentially coats triacylglycerol-rich droplets, and its abundance tracks triacylglycerol rather than sterol content; in Plin2-null liver, reduced triacylglycerol coincides with increased cholesteryl esters. (14) A droplet population that is cholesteryl-ester-rich but triglyceride-poor would thus be expected to carry comparatively little PLIN2, exactly as observed in F6. Moreover, because PLIN2 protects droplets from lipolytic turnover, a low-PLIN2 droplet pool is also likely to be more dynamic and less stable (19) suggesting that the F6 droplets differ from control droplets not only in core lipid composition but potentially in turnover.

These findings are consistent with reports that *Scarb2*-deficient mice show reduced lipid storage in adipose tissue and liver (18): on a triglyceride basis our data agree, as F6 also had the lowest triglyceride content. Rather than abolishing storage, however, LIMP-2 loss appears to redirect it from triglyceride towards a cholesterol/cholesteryl-ester pool — a qualitative shift in stored lipid identity.

4.3 A compensatory lysosomal response and possible enzyme cross-talk

The modest increase in LAMP1 in both mutants is consistent with a compensatory lysosomal response to disruption of the GCase–LIMP-2 axis, as has been described in GCase-deficient models where impaired enzyme activity is accompanied by increased lysosomal content and altered lysosomal morphology. (20) Given that the present densitometry did not reach statistical significance, this is interpreted cautiously as a directional trend that may be corroborated, or refined, by lysosomal imaging in future work.

The accumulation of glucosylceramide and glucosylated sterol in the GCase-deficient line also raises the question of enzymatic compensation. The non-lysosomal glucosylceramidase GBA2 shares substrate specificity with GCase, and genetic studies indicate cross-talk between the two enzymes, with up-regulation of GBA2 and partial functional compensation upon loss of GCase. (12) Whether GBA2 is up-regulated in 11F cells could be addressed directly by measuring GBA2 expression and activity and represents a logical next step for this work.

4.4 Limitations

Several limitations temper these conclusions. The Western blot and imaging analyses rest on three independent biological replicates per condition, and a number of the directional changes discussed above — including the reduction of GBA1 in 11F, the PLIN2 gradient, the LAMP1 elevation, and the F6-versus-CTRL increase in lipid-droplet burden — did not reach formal statistical significance under one-way ANOVA with multiple-comparison correction. Because these changes are nevertheless consistent across the Western blot, imaging and lipidomic datasets, they are reported here as concordant biological trends; larger replicate numbers would be required to establish them as statistically robust. Inferential statistics on lipid-droplet morphometry were restricted to per-image summary values to avoid pseudoreplication arising from the pooling of thousands of individual droplets.

A further consideration concerns the validation of the F6 line at the protein level. As noted in Section 4.1, the LIMP-2 Western blot could not be used owing to contamination of the F6 lane by WT signal, and F6 LIMP-2 deficiency should therefore be confirmed by an independent method — for example a repeat immunoblot with a clean lane layout, quantitative PCR of *SCARB2*, or a functional readout of LIMP-2-dependent trafficking. Importantly, the F6-specific lipidomic phenotype (accumulation of free cholesterol and cholesteryl esters, lowest triglycerides) is in the direction expected for a functional LIMP-2 deficiency and provides independent support for the integrity of the line at the lipid-metabolism level.

Finally, the use of a HEK293 model, while well suited to dissecting the GCase–LIMP-2 relationship, does not capture the neuronal context in which these pathways are most relevant to disease, and extension to neuronal models would strengthen the translational interpretation.

5. Conclusion

This study set out to clarify the roles of GBA1 and LIMP-2 in cellular lipid homeostasis, using wild-type, GBA1-knockout (11F) and SCARB2-knockout (F6) HEK293 cells characterised in parallel by Western blotting, lipid-droplet imaging and targeted lipidomics. Bringing the three approaches together produced a consistent picture in which loss of GBA1 and loss of LIMP-2 perturb lipid-droplet homeostasis through two distinct, mechanism-specific routes rather than through a single shared pathway.

GBA1 deficiency was associated with the accumulation of glucosyl/galactosylceramides and glucosylated cholesterol, together with significantly smaller lipid droplets, a reduced triglyceride load and correspondingly lower PLIN2 — a profile consistent with loss of GCase hydrolytic activity and its downstream effects on glycosphingolipid and neutral-lipid metabolism. LIMP-2 deficiency, by contrast, drove an accumulation of lipid droplets that were richer in free cholesterol and cholesteryl esters yet lower in triglyceride and coated by comparatively little PLIN2 — a signature consistent with the GCase-independent role of LIMP-2 in lysosomal cholesterol export. The lipidomic data were central to this interpretation: they independently confirmed GCase loss-of-function in the 11F line and resolved the apparent paradox of increased droplet number alongside reduced PLIN2 in F6 by revealing the underlying shift towards a cholesterol- and cholesteryl-ester-rich droplet population. Together, these findings support a model of GCase-dependent and GCase-independent contributions of the GCase–LIMP-2 axis to lipid-droplet biology.

These conclusions should be regarded as well-supported but preliminary: several of the biochemical and morphometric differences represented consistent trends that did not reach statistical significance at three biological replicates, the F6 line still requires independent confirmation of LIMP-2 deficiency at the protein level, and the observations were made in a HEK293 model rather than in neuronal cells. Future work — increasing replicate numbers, validating the F6 line, measuring GBA2 as a candidate compensatory enzyme, and extending the analysis to neuronal systems — would consolidate and build on these results. Nonetheless, by linking two distinct lysosomal lesions to specific and separable changes in lipid-droplet composition, this work contributes to a mechanistic understanding of how lysosomal dysfunction reshapes cellular lipid storage, a process of direct relevance to Gaucher disease and to GBA1-associated neurodegeneration.

Bibliography

1. Braulke T, Bonifacino JS. Sorting of lysosomal proteins. Biochim Biophys Acta BBA - Mol Cell Res. 2009 Apr;1793(4):605–14. doi:10.1016/j.bbamcr.2008.10.016

2. Dobert JP, Schäfer JH, Dal Maso T, Ravindran P, Huard DJE, Socher E, et al. Cryo-TEM structure of β-glucocerebrosidase in complex with its transporter LIMP-2. Nat Commun. 2025 Mar 30;16(1):3074. doi:10.1038/s41467-025-58340-1

3. Boustany RMN. Lysosomal storage diseases—the horizon expands. Nat Rev Neurol. 2013 Oct;9(10):583–98. doi:10.1038/nrneurol.2013.163

4. Reczek D, Schwake M, Schröder J, Hughes H, Blanz J, Jin X, et al. LIMP-2 Is a Receptor for Lysosomal Mannose-6-Phosphate-Independent Targeting of β-Glucocerebrosidase. Cell. 2007 Nov;131(4):770–83. doi:10.1016/j.cell.2007.10.018

5. Aflaki E, Westbroek W, Sidransky E. The Complicated Relationship between Gaucher Disease and Parkinsonism: Insights from a Rare Disease. Neuron. 2017 Feb;93(4):737–46. doi:10.1016/j.neuron.2017.01.018

6. Migdalska-Richards A, Schapira AHV. The relationship between glucocerebrosidase mutations and Parkinson disease. J Neurochem. 2016 Oct;139(S1):77–90. doi:10.1111/jnc.13385

7. Chatterjee D, Krainc D. Mechanisms of Glucocerebrosidase Dysfunction in Parkinson's Disease. J Mol Biol. 2023 Jun;435(12):168023. doi:10.1016/j.jmb.2023.168023

8. Neculai D, Schwake M, Ravichandran M, Zunke F, Collins RF, Peters J, et al. Structure of LIMP-2 provides functional insights with implications for SR-BI and CD36. Nature. 2013 Dec 5;504(7478):172–6. doi:10.1038/nature12684

9. Zunke F, Andresen L, Wesseler S, Groth J, Arnold P, Rothaug M, et al. Characterization of the complex formed by β-glucocerebrosidase and the lysosomal integral membrane protein type-2. Proc Natl Acad Sci. 2016 Apr 5;113(14):3791–6. doi:10.1073/pnas.1514005113

10. Rudnik S, Heybrock S, Coyaud E, Xu Z, Neculai D, Raught B, et al. The lysosomal lipid transporter LIMP-2 is part of lysosome–ER STARD3-VAPB-dependent contact sites. J Cell Sci. 2024 Nov 15;137(22):jcs261810. doi:10.1242/jcs.261810

11. Heybrock S, Kanerva K, Meng Y, Ing C, Liang A, Xiong ZJ, et al. Lysosomal integral membrane protein-2 (LIMP-2/SCARB2) is involved in lysosomal cholesterol export. Nat Commun. 2019 Aug 6;10(1):3521. doi:10.1038/s41467-019-11425-0

12. Yildiz Y, Hoffmann P, Vom Dahl S, Breiden B, Sandhoff R, Niederau C, et al. Functional and genetic characterization of the non-lysosomal glucosylceramidase 2 as a modifier for Gaucher disease. Orphanet J Rare Dis. 2013;8(1):151. doi:10.1186/1750-1172-8-151

13. Marques ARA, Mirzaian M, Akiyama H, Wisse P, Ferraz MJ, Gaspar P, et al. Glucosylated cholesterol in mammalian cells and tissues: formation and degradation by multiple cellular β-glucosidases. J Lipid Res. 2016 Mar;57(3):451–63. doi:10.1194/jlr.M064923

14. Doncheva AI, Li Y, Khanal P, Hjorth M, Kolset SO, Norheim FA, et al. Altered hepatic lipid droplet morphology and lipid metabolism in fasted Plin2-null mice. J Lipid Res. 2023 Dec;64(12):100461. doi:10.1016/j.jlr.2023.100461

15. Navarro-Romero A, Fernandez-Gonzalez I, Riera J, Montpeyo M, Albert-Bayo M, Lopez-Royo T, et al. Lysosomal lipid alterations caused by glucocerebrosidase deficiency promote lysosomal dysfunction, chaperone-mediated-autophagy deficiency, and alpha-synuclein pathology. Npj Park Dis. 2022 Oct 6;8(1):126. doi:10.1038/s41531-022-00397-6

16. Brekk OR, Honey JR, Lee S, Hallett PJ, Isacson O. Cell type-specific lipid storage changes in Parkinson's disease patient brains are recapitulated by experimental glycolipid disturbance. Proc Natl Acad Sci. 2020 Nov 3;117(44):27646–54. doi:10.1073/pnas.2003021117

17. Tahanis A, Nguyen T, Oji S, Martinez De Kraatz M, Jayasi J, Anderson M, et al. Glucocerebrosidase Deficiency Dysregulates Human Astrocyte Lipid Metabolism [Internet]. Neuroscience; 2025 [cited 2026 Jul 5]. Available from: http://biorxiv.org/lookup/doi/10.1101/2025.01.09.632210 doi:10.1101/2025.01.09.632210

18. Zou Y, Pei J, Wang Y, Chen Q, Sun M, Kang L, et al. The Deficiency of SCARB2/LIMP-2 Impairs Metabolism via Disrupted mTORC1-Dependent Mitochondrial OXPHOS. Int J Mol Sci. 2022 Aug 3;23(15):8634. doi:10.3390/ijms23158634

19. Loix M, Wouters E, Vanherle S, Dehairs J, McManaman JL, Kemps H, et al. Perilipin-2 limits remyelination by preventing lipid droplet degradation. Cell Mol Life Sci. 2022 Oct;79(10):515. doi:10.1007/s00018-022-04547-0

20. Magalhaes J, Gegg ME, Migdalska-Richards A, Doherty MK, Whitfield PD, Schapira AHV. Autophagic lysosome reformation dysfunction in glucocerebrosidase deficient cells: relevance to Parkinson disease. Hum Mol Genet. 2016 Aug 15;25(16):3432–45. doi:10.1093/hmg/ddw185